BINDER CONTENT AND STORING CONDITIONS OF INORGANICALLY-BOUND FOUNDRY CORES DETERMINE THE INTENSITY AND ONSET TIME OF GAS RELEASE IN METAL CASTING

Simon Kammerloher [ORCID], **Benedikt Kirchebner, Erwin Reberger, Christoph Weidner, Wolfram Volk and Philipp Lechner**

Department of Mechanical Engineering, TUM School of Engineering and Design, Chair of Metal Forming and Casting, Technical University of Munich, Munich, Germany

Abstract

Organically-bound foundry cores are substituted by inorganically-bound cores increasingly. This trend is due to regulatory efforts, workplace safety issues, and increasing costs for waste deposits. Changing the binder system reduces the emissions to mostly water vapor, solving health and safety issues. Yet, the difference in the behavior of the gas phase, namely, the condensation potential of water, changes the casting process drastically. In contrast with the continuous generation and discharge of combustion products in the case of organic binders, water accumulates within the foundry core. Only once the cold spots of the core reach boiling temperature noteworthy amounts of vapor are created, increasing the chance for gas defects of the cast parts. Countermeasures have to be taken when designing the core's geometry. We conducted the following research to improve the understanding of core gas release and its interactions with the foundry core's binder content and storage conditions. Both binder content and relative humidity during storage were varied in three steps. Their influence on the core gas amount, time of gas generation, and gas permeability of the cores were investigated. The experiments were performed in the institute's Induction Analysis Furnace and an aluminum melt bath. We found a strong dependency of storage humidity, further increased by increasing binder content on the gas amount and time of the gas release.

Keywords: *foundry core, inorganic binder, organic binder, core gas, permeability, core shooting*

Introduction

Expendable molds and foundry cores are mostly made from bonded sand. Organic substances are well known as bonding agents.[1,2] Commonly used organic binders are furans, alkaline phenolics, and phenol–urethanes.[3] In addition to contributing to CO_2 emissions, this type of binder releases toxic fumes due to heat degradation.[4] The effects are air-polluting, toxic, carcinogenic, and mutagenic. An in-depth analysis of the decomposition products of organic binders is described, e.g., in (Reference [5]). In contrast, inorganic water glass binders release water vapor.[6] Due to the implementation organic additives, harmful decomposition products occur on a far smaller scale.[7] Thus, inorganic binders are increasingly used due to legal regulations and work safety considerations.[8] As always, changing to a different material in production poses new challenges. With molds and cores, the most prominent changes from organic to inorganic are their different susceptibility to mechanical deterioration due to humidity[9] and their decoring behavior.[10] Another aspect that needs consideration when designing cast products is the materials' difference in gas generation. With inorganic binders, water evaporates in the hot outer shell first during casting and condenses in the cooler parts of the core. This leads to an increase in local water content within the core during casting. The accumulated water evaporates as soon as the core's center reaches boiling temperature and needs to leave the core quickly when pressure build-up should be avoided. With organic binders, whose solvents are more volatile and less concentrated, almost all the reaction products leave the core continually through the core

Simon Kammerloher and Benedikt Kirchebner have contributed equally to this work.
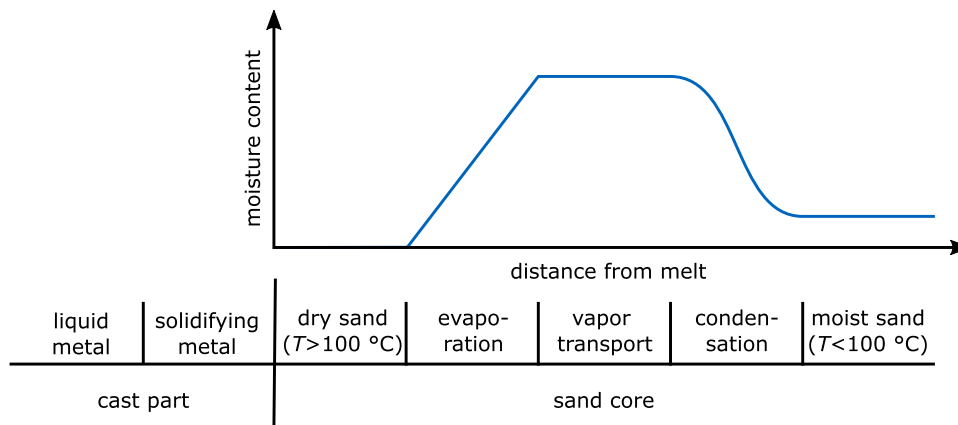
Figure 1. *Schematic of the water transport in inorganic foundry cores due to heat input from the melt.*[12]

bearings, also called core prints. This reduces the chance of pressure building up and forcing gas into the melt, resulting in casting defects.[11] Knowledge of the behavior of inorganically-bound foundry cores is essential to increase process stability in the casting industry. Hence, a material model for the gas release of those cores could assist in optimizing the designing process to avoid blowholes. Our goal was to develop insight into the correlations between process and storing parameters on the one hand with the core gas amount, time of gas release, and gas permeability of the cores on the other hand. The measurements performed within this research shall build the foundation for the material model. Herein, we continue and expand our work as shown in (Reference 12).

Theoretical Background

Moisture Transport in Foundry Cores

The binders of foundry cores release various substances due to the heating effect of the melt. Organic binders decompose and mostly form gaseous products.[13] Inorganic binders, on the other hand, release mostly water vapor, which condenses upon reaching regions of sand at temperatures below 100 °C. This reduces the amount of gas present in the core, counteracting gas generation and thus preventing venting of the core at the early stages of the casting process due to a lack of pressure increase. Accordingly, gas transport must be considered on top of gas generation to study porosity caused by gas escape.[14] In the outer shell area of a foundry core, surrounded by melt, the temperature rises above 100 °C. The water in this area evaporates, increasing in volume. Due to the counterpressure of the melt, the water vapor moves toward the core's center, pushing air outward through the core bearings. Once the steam reaches an area within the core of a temperature below 100 °C, it will condense, releasing heat to the surrounding material. Hence, heat is transported within

the core due to conduction and convection phenomena in the molding material.[14] These effects lead to an area of increasing moisture content traveling toward the core's center. Its traveling path can be divided into five distinct zones, shown schematically in Figure 1:[14]

- *Dry sand zone*: temperature > 100 °C, all moisture evaporated
- *Evaporation zone*: temperature = 100 °C, moisture is evaporating
- *Vapor transport zone*: temperature = 100 °C, steam is passing through
- *Condensation zone*: temperature < 100 °C, steam condenses, and moisture increases
- *Moist sand zone*: temperature < 100 °C, unaffected by moisture transport, yet

Gas Shock

In the early stages of the casting process, moisture is transported toward the core's center, as described above. Due to the continuous re-condensation, no pressure builds up in the core. Hence, very little water is transported out of the core but accumulates in its coldest areas.[14] Once those now wet, cold spots within the core reach boiling temperature, the accumulated water evaporates quickly due to its small spatial extent. Hence, the pressure within the core rises, overcoming the counterpressure of the melt if not appropriately vented through the core's bearings. The gas bubbles traveling through the melt can lead to gas porosity, blowholes, and subsequently to scrap parts.[11] This abrupt evaporation and escape of the core's moisture is called gas shock. To prevent blowholes in the cast part, either the melt surrounding the core has to solidify before the gas shock occurs, or the core's geometry has to be designed in a way as to allow the vapor to escape via its bearings.

Materials and Methods

Specimens

In this work, silica sand with a mean grain diameter of .32 mm is used (H32, Quarzwerke GmbH, Germany). A two-component inorganic binder system is added (INOTEC EP 4158 and INOTEC PROMOTOR TC 4500, ASK Chemicals, Germany). The binder system is used in three different quantities of 2.0, 2.5, and 3.0 wt% binder and 1.6, 2.0, and 2.4 wt% promoter, respectively. For the experiments, three different geometries of specimens were used. All of which were cylindrical with length and outer diameter of 50 mm. One version was made entirely of sand, the other two had graphite tubes of 5.0- and 12.5-mm wall thickness forming the outer diameter. Therefore, the sand filling these tubes featuring diameters of 40 and 25 mm, respectively.

According to (Reference [12]), the dry specimens' average density is 1.59 g/cm^3, resulting in specimen weights of 159.2, 99.9, and 39.0 g. Considering the density of silicon dioxide, the sand's bulk material, of 2.65 g/cm^3, the specimens consist of 60% sand and 40% air.

The specimens were produced via the core shooting process in a Loramendi SLC2-25L (Loramendi S.Coop., Spain). The mold's cavity resembles the pure sand specimen. In the other cases, the graphite tubes were inserted into the cavity, thus reducing the cavity's open diameter. The core shooting parameters are shown in Table 1.

After core shooting, the specimens were stored in a climate cabinet for at least 24 h to homogenize their moisture content. The set temperature was 20 °C, and relative humidity (RH) was varied in three steps at 10, 50, and 90%

Induction Analysis Furnace (IAF)

Both the core gas creation and the gas permeability test were performed using the institute's Induction Analysis Furnace (IAF), described in (Reference [12]). This is a highly controllable test stand regarding atmosphere and temperature. Its test chamber consists of an aluminum cube with an inner edge length of roughly 200 mm. By adjusting the argon flow into and out of the test chamber, volumetric flow, pressure, and oxygen levels are controlled. The aluminum side plates are water-cooled. The specimen is suspended in the cube's center, surrounded by an induction coil. An in-depth description of the IAF is provided in (Reference [12]). Twelve-core gas creation is tested by closing the graphite tube on both ends, except a heated copper pipe, leading into a water reservoir situated on a laboratory scale (XSR304, Mettler-Toledo GmbH, Germany). Once the specimen gets heated, water evaporates inside the sand specimen and condenses in the water

Table 1. Core Shooting Process Settings

Parameter	Value
Tool temperature	150 °C
Shooting pressure	5 bar
Shooting time	1 s
Gassing temperature	220 °C
Pre-gassing time	10 s
Gassing time	5 s

Figure 2. Specimen geometry and composition.[12]

reservoir, increasing its weight. A heating rate of 50 °C/min was applied to the surface until 800 °C were reached, then the temperature was held constant for 5 min.

The data of the sample's weight were smoothed and detrended to rid it of influences of gas bubbles leaving the copper pipe and mass reduction due to evaporation.[12] The result is a curve with two steady states, one at the beginning and another toward the end of the experiment, and an increase in weight in between, representing the gas release from the specimen. The change in the signal, representing the time of gas release, is evaluated using two approximating segments assessed by a cost function according to (Reference [15]). The sand specimens with the smallest diameter were installed in the test chamber to measure gas permeability. The lower end of the graphite tube was left uncovered toward the test chamber, while the upper end was connected to a copper pipe leading into the open. Argon flow is detected via a flow meter on the outlet (SFAH-100U-Q8S-PNL, Festo Vertrieb GmbH and Co. KG, Germany). The pressure inside the test chamber was gradually increased by approximately 7 mbar/s up to 0.4 bar.

Moisture Balance

A KERN DBS 60-3 moisture balance (KERN and SOHN GmbH, Germany) is used to validate the experimental results of the core gas creation within the IAF. For this, a projecting smaller cylinder on the outlet surface of the specimen cylinder due to the core shooting process is filed off. This is visualized by the scetch in Figure 2. On the balance, the sand is heated to 200 °C, using radiation. The
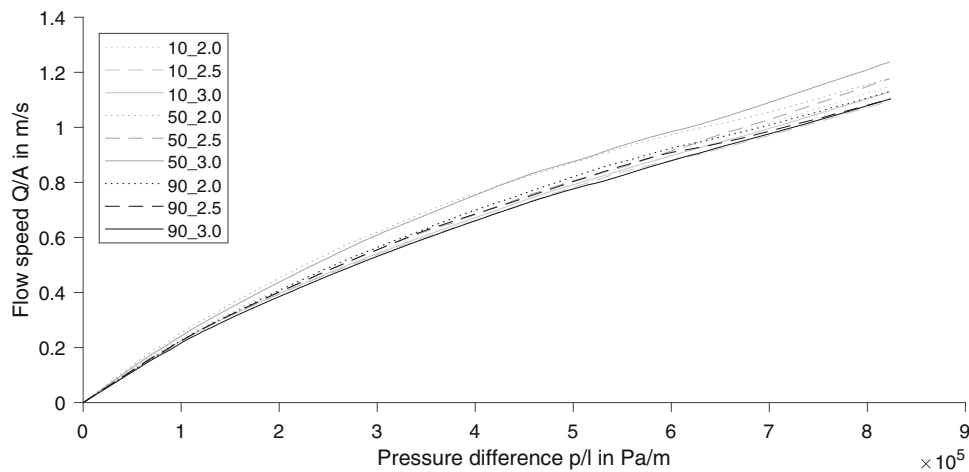
Figure 3. Gas permeability measurements. The flow speed Q/A is shown with respect to the sample length-specific pressure difference p/l.

temperature is gradually raised and remains at its maximum for 5 min. The signal is logged via the scales RS232 interface.

Submersion Experiments

The largest sand cylinders were submerged in molten aluminum (AlSi12) at 750 °C. For that, an A20 clay–graphite crucible was placed in a resistance-heated furnace, K4-13 (Nabertherm, Germany), until the desired temperature was reached. Before each experiment, the melt surface was skimmed. A specimen was gripped with hot pliers, holding it at two spots on the cylindrical surface to minimize the effects of the tooling. The specimen was then submerged in the melt. A camera recorded the melt's surface during the experiment, so core gas bubbles could be detected, hence timing the start of the gas shock. After the experiment, the melt was given time to regain its starting temperature.

Results and Discussion

Three repetitions of the experiments obtain the values in the figures below. Both the values and their standard deviations are shown in tables in Appendix 1.

Gas Permeability

The results of the gas permeability measurements are shown in Figure 3. The legend lists the RH values, followed by the binder content. The measured values were transformed to eliminate the specimen's geometric aspects. The pressure (p) is expressed per length (l) and the volumetric flow (Q) per cross-sectional area (A).

Each line represents the average of three specimens with identical values regarding relative humidity during storage and binder content. The data are subject to high variation. Hence, the influence of the process parameters on gas permeability is low. Yet, the specimens with higher binder content tend to show less gas permeability than the others. Both the 10 and 90% RH samples make up the bulk of lines in the lower segment, whereas the specimens stored at 50% RH sit slightly above those.

Moisture Balance

The measuring results of the moisture balance are shown in Figure 4. Water content in the sand specimens shows an exponential increase with increasing relative humidity during storage. An increase in water content with increasing binder content is apparent as well. Specimens stored at 10% RH contain between 0.2 and .3% water, according to their binder content. Whereas specimens stored at 90% RH show between 0.9 and 1.2% water content. The binder structure covering the grains of sand provides the potential for water to attach to the material in higher quantities. The water content of the specimen and the specific volume of saturated steam of 1.7 l/g at 100 °C and atmospheric pressure results in a volume of water vapor created between 0.3 and 2.0 l. Hence, filling the specimen's pore volume between 12- and 80-fold. Therefore, after the first bit of gas leaves the specimen, the atmosphere within is mostly water vapor.

Gas Shock in IAF

The measurements of water release in the IAF, presented in Figure 5, show similar behavior as those on the moisture balance. Yet again, total water content increases exponentially with respect to RH in storage. Also, the difference between 2.0 and 3.0 wt% increases with increasing RH.
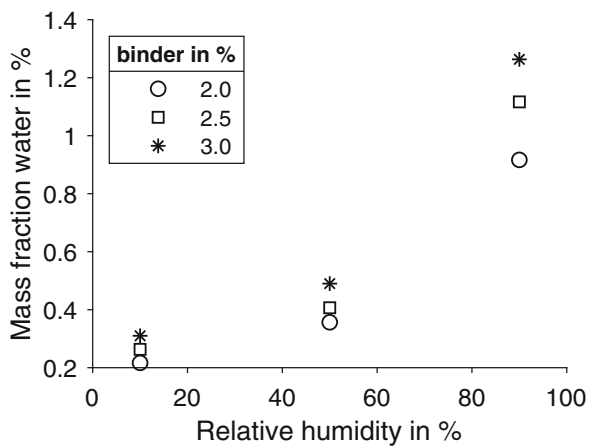
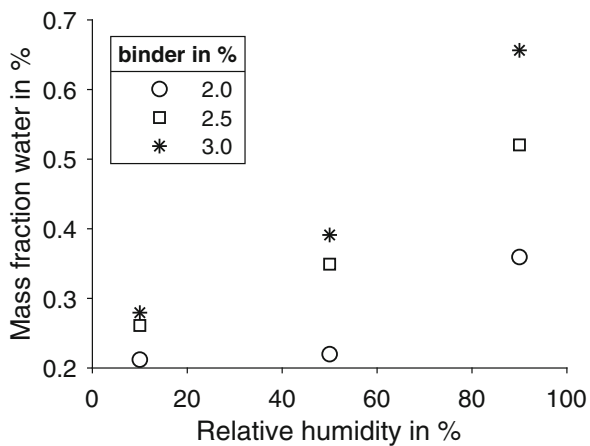**Figure 4. Water content as per moisture balance depending on binder content and relative humidity at 20 °C.**
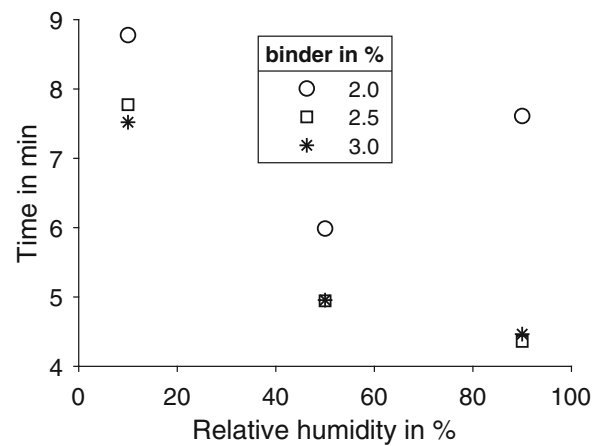

Figure 6. Time after the start of the experiment at which gas release from the specimen is most prominent for a heating rate of 50 °C/min, using specimens of 40-mm diameter inside graphite tube.

Figure 5. Water content as per IAF depending on binder content and relative humidity at 20 °C.
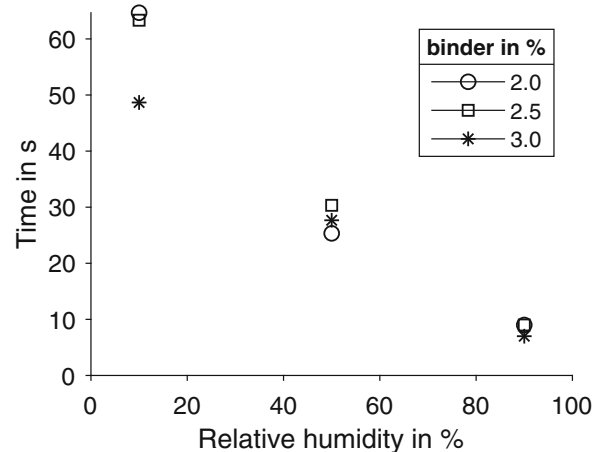

Figure 7. Time after submersion in aluminum melt at which gas release from the specimen starts, using specimens of 50-mm diameter without graphite tube.

Although the total water content of the specimens stored at 10% RH is identical between 0.2 and .3%, the maximum water content only reaches about half the amount of the results on the moisture balance. This is likely due to the difference in composition of both specimens, as the ones on the moisture balance contain a higher fraction of rim material. As the sand is compressed against the tool here, a different structure and alignment of grains might cause differing interactions with water.

When evaluating the time of gas shock, as shown in Figure 5, a reduced delay with increased RH in storage is apparent. Also, higher binder content and therefore increased amounts of water within the specimen tend to reduce the delay time of gas release. The data point representing 2.0% binder at 90% RH seems to be an outlier. Those effects are probably due to two leading causes. For one, heat conductivity in foundry cores is significantly increased with vapor movement within them. Hence, heating the middle of the specimen quicker. Also, water accumulates in the cold center of the specimen by

repetitive evaporation and condensation. Once the channels between the sand grains are filled with water, this is no longer possible, and vapor would be forced out of the core and be detected via the scales.

Submersion Experiments

Figure 7 shows the submersion time at the onset of the gas shock. A very similar relation between storage RH and the time of the gas, as in the experiments in the IAF, is apparent. The onset times shift to values between 10 and 70 s due to the difference in heating. Yet again, the delay decreases with increasing RH. The binder content seems to be of greater influence for lower RH, relatively increasing the amount of chemically bound water.

Conclusion

Due to environmental and work safety regulations, the use of inorganically-bound foundry cores is increasing. Their reaction products, being mostly water, offer new challenges. Due to moisture transport toward the cool spots in the core's center, the final gas generation is rather rapid and tends to create blowholes within the cast part. We were able to quantify the water amount released over time from the core in relation to both binder content and relative humidity at storage. The data created within the IAF matches that received via moisture balance and submersion of cores into the melt, as well as to values given in the literature. In addition, gas permeability was measured for a pressure difference of up to 0.4 bar. An increase in the binder content of inorganically-bound foundry cores makes them more susceptible to moisture exposure during storage, allowing them to absorb more water. Relative humidity also plays a big role in how much water the core absorbs. Both factors lead to a higher and earlier gas release from the core when heated up. The next step will be to build a material model to predict gas release and help design foundry cores and casting processes.

Open Access

Appendix 1

See Tables 2, 3, 4, 5 and 6.

Table 2. Gas permeability as shown in Figure 3

Q/A in m/s at 1e5 Pa/m	10% RH	50% RH	90% RH
2.0% binder	0.23	0.25	0.22
2.5% binder	0.23	0.22	0.22
3.0% binder	0.22	0.24	0.22
Std. in m/s			
2.0% binder	0.01	0.01	0.01
2.5% binder	0.01	0.02	0.03
3.0% binder	0.02	0.00	0.02
Q/A in m/s at 3e5 Pa/m	10% RH	50% RH	90% RH
2.0% binder	0.56	0.62	0.56
2.5% binder	0.54	0.55	0.56
3.0% binder	0.54	0.61	0.53
Std. in m/s			
2.0% binder	0.01	0.01	0.04
2.5% binder	0.01	0.05	0.06
3.0% binder	0.04	0.01	0.05
Q/A in m/s at 5e5 Pa/m	10% RH	50% RH	90% RH
2.0% binder	0.82	0.87	0.82
2.5% binder	0.78	0.81	0.80
3.0% binder	0.79	0.88	0.78
Std. in m/s			
2.0% binder	0.01	0.03	0.06
2.5% binder	0.02	0.07	0.07
3.0% binder	0.06	0.02	0.07
Q/A in m/s at 7e5 Pa/m	10% RH	50% RH	90% RH
2.0% binder	1.02	1.06	1.01
2.5% binder	0.97	1.03	0.99
3.0% binder	1.00	1.09	0.98
Std. in m/s			
2.0% binder	0.01	0.04	0.07
2.5% binder	0.02	0.11	0.07
3.0% binder	0.09	0.07	0.10

Table 3. Water content as per moisture balance depending on binder content and relative humidity as shown in Figure 4

Water content in %	10% RH	50% RH	90% RH
2.0% binder	0.22	0.36	0.92
2.5% binder	0.26	0.41	1.12
3.0% binder	0.31	0.49	1.26
Std. in ‰			
2.0% binder	0.12	0.12	1.10
2.5% binder	0.25	0.21	0.80
3.0% binder	0.10	0.17	0.55

Table 4. Water content as per IAF depending on binder content and relative humidity as shown in Figure 5

Water content in %	10% RH	50% RH	90% RH
2.0% binder	0.21	0.22	0.36
2.5% binder	0.26	0.35	0.52
3.0% binder	0.28	0.39	0.66
Std. in ‰			
2.0% binder	0.37	0.42	1.36
2.5% binder	0.13	0.69	0.18
3.0% binder	0.12	0.22	0.90

Table 5. Time after start of the experiment at which gas release from the specimen is most prominent for a heating rate of 50 °C/min as per IAS as shown in Figure 6

Time in min	10% RH	50% RH	90% RH
2.0% binder	8.78	5.99	7.61
2.5% binder	7.77	4.94	4.36
3.0% binder	7.52	4.96	4.46
Std. in min			
2.0% binder	0.74	0.69	2.64
2.5% binder	0.03	0.98	0.71
3.0% binder	0.24	0.20	0.14

Table 6. Time after submersion in aluminum melt at which gas release from the specimen starts as shown in Figure 7

Time in s	10% RH	50% RH	90% RH
2.0% binder	65	25	9
2.5% binder	63	30	9
3.0% binder	49	28	7
Std. in s			
2.0% binder	2.5	12.7	1.4
2.5% binder	1.5	8.7	2.6
3.0% binder	2.5	11.4	1.4

REFERENCES

1. S.G. Acharya, J.A. Vadher, M. Sheladiya, A furan no-bake binder system analysis for improved casting quality. Int. J. Metalcast. **10**(4), 491–499 (2016). https://doi.org/10.1007/s40962-016-0059-x
2. S. Saetta, V. Caldarelli, Lean production as a tool for green production: the green foundry case study. Proced. Manuf. **42**, 498–502 (2020). https://doi.org/10.1016/j.promfg.2020.02.042
3. P. Wan, J. Zhou, Y. Li, Y. Yin, X. Peng, X. Ji, X. Shen, Kinetic analysis of resin binder for casting in combustion decomposition process. J. Therm. Anal. Calorim. **147**(11), 6323–6336 (2022). https://doi.org/10.1007/s10973-021-10902-3
4. H. Polzin, *Inorganic Binders: For Mould and Core Production in the Foundry*, 1st edn. (Schiele & Schön, Berlin, 2014)
5. M. Kubecki, M. Holtzer, A. Bobrowski, R. Dańko, B. Grabowska, S. Żymankowska-Kumon, Analysis of the compounds from the btex group, emitted during thermal decomposition of alkyd resin. Arch. Foundry Eng. **12**(3), 69–74 (2012). https://doi.org/10.2478/v10266-012-0084-z
6. A. Siewiorek, R. Nowaka, A. Chojeckib, J. Mocek, Gas evolution rate from heated moulding sands bonded with organic binders. Arch. Foundry Eng. **11**(1), 87–92 (2011)
7. A. Bobrowski, M. Holtzer, S. Żymankowska-Kumon, R. Dańko, Harmfulness assessment of moulding sands with a geopolymer binder and a new hardener, in an aspect of the emission of substances from the btex group. Arch. Metall. Mater. **60**(1), 341–344 (2015). https://doi.org/10.1515/amm-2015-0056
8. E. Weissenbek, J. Willimayer, J. Wolf, Bmw-leicht-metallgießerei setzt auf anorganisch gebundene kerne. Gießerei **95**(6), 30–33 (2008)
9. P. Lechner, C. Hartmann, F. Ettemeyer, W. Volk, A plane stress failure criterion for inorganically-bound core materials. Materials **14**(2), 247 (2021). https://doi.org/10.3390/ma14020247
10. F. Ettemeyer, M. Schweinefuß, P. Lechner, J. Stahl, T. Greß, J. Kaindl, L. Durach, W. Volk, D. Günther, Characterisation of the decoring behaviour of inorganically bound cast-in sand cores for light metal casting. J. Mater. Process. Technol. **296**, 117201 (2021). https://doi.org/10.1016/j.jmatprotec.2021.117201
11. R. Monroe, Porosity in castings. ChemInform. (2006). https://doi.org/10.1002/CHIN.200642218
12. B. Kirchebner, S. Kammerloher, G. Fuchs, E. Reberger, W. Volk, P. Lechner, A test stand for quantifying the core gas release and the gas permeability of inorganically-bound foundry cores. Int. J. Metalcast. 1–9 (2023)
13. P. Wan, J. Zhou, Y. Li, Y. Yin, D. Huang, X. Ji, X. Shen, Experimental study on gas evolution process of binders in foundry industry based on tg-ms. Proced.

Manuf. **37**, 311–318 (2019). https://doi.org/10.1016/j. promfg.2019.12.053

14. J. Campbell, *Complete Casting Handbook: Metal Casting Processes, Techniques and Design*, 1st edn. (Butterworth-Heinemann, Oxford, 2011)

15. R. Killick, P. Fearnhead, I.A. Eckley, Optimal detection of changepoints with a linear computational cost. J. Am. Stat. Assoc. **107**(500), 1590–1598 (2012)